Your Data Is Not Perfect: Towards Cross-Domain Out-of-Distribution Detection in Class-Imbalanced Data

Xiang Fang (Corresponding author, Email: xiang003@e.ntu.edu.sg)[a,b,c],
Arvind Easwaran (Email: arvinde@ntu.edu.sg)[b,c], Blaise Genest (Email:
blaise.genest@cnrsatcreate.sg)[c], Ponnuthurai Nagaratnam Suganthan
(Email: p.n.suganthan@qu.edu.qa)[d]

[a]*Interdisciplinary Graduate Programme-Energy Research Institute @ NTU, Nanyang Technological University, Singapore*
[b]*College of Computing and Data Science, Nanyang Technological University, Singapore*
[c]*CNRS and CNRS@CREATE, IPAL IRL 2955, France and Singapore*
[d]*KINDI Computing Research Center, College of Engineering, Qatar University, Doha, Qatar*

Abstract

Out-of-distribution detection (OOD detection) aims to detect test samples drawn from a distribution that is different from the training distribution, in order to prevent models trained on in-distribution (ID) data from providing unavailable outputs. Current OOD detection systems typically refer to a single-domain class-balanced assumption that both the training and testing sets belong to the same domain and each class has the same size. Unfortunately, most real-world datasets contain multiple domains and class-imbalanced distributions, which severely limits the applicability of existing works. Previous OOD detection systems only focus on the *semantic* gap between ID and OOD samples. Besides the *semantic* gap, we are faced with two additional gaps: the *domain* gap between source and target domains, and the *class-imbalance* gap between different classes. In fact, similar objects from different domains should belong to the same class. In this paper, we introduce a realistic yet challenging setting: class-imbalanced cross-domain OOD detection (CCOD), which contains a well-labeled (but usually small) source set for training and conducts OOD detection on an unlabeled (but usually larger) target set for testing. We do not assume that the target domain contains only OOD classes or that it is class-balanced: the distribution among classes of the target dataset need not be the same as the source dataset. To tackle this challenging setting with an OOD detection system, we pro-

pose a novel uncertainty-aware adaptive semantic alignment (UASA) network based on a prototype-based alignment strategy. Specifically, we first build label-driven prototypes in the source domain and utilize these prototypes for target classification to close the domain gap. Rather than utilizing fixed thresholds for OOD detection, we generate adaptive sample-wise thresholds to handle the semantic gap. Finally, we conduct uncertainty-aware clustering to group semantically similar target samples to relieve the class-imbalance gap. Extensive experiments on three challenging benchmarks (Office-Home, VisDA-C and DomainNet) demonstrate that our proposed UASA outperforms state-of-the-art methods by a large margin.

Keywords: Out-of-distribution detection, Multi-domain alignment, Class-imbalanced data, Label-driven prototype building, Prototype-guided domain alignment, Adaptive threshold generation, Uncertainty-aware target clustering

1. Introduction

With the successful development of deep learning, deep neural networks (DNNs) (Reimers et al., 2020; De and Pedersen, 2021; Vellido et al., 1999; Yahia et al., 2000) have been widely applied to many expert and intelligent systems (Atmakuru et al., 2024; Maqsood et al., 2024; Wang et al., 2025) based on a closed-set assumption that all the test samples are known during training (Luo et al., 2024; Jiao et al., 2024; Li et al., 2024; Neal et al., 2018; Cho and Choo, 2022). Unfortunately, real-world datasets contain many outliers that are difficult to distinguish. These outliers are called as out-of-distribution (OOD) samples, while these non-outliers are treated as in-distribution (ID) samples. In fact, standard DNN-based systems compulsorily classify both ID and OOD samples as belonging to one of the known classes (Yao et al., 2024; Rastegari et al., 2016; Zhang et al., 2022; Du et al., 2020). The wrong classification of outliers will result in irrecoverable losses in some safety-critical systems, such as autonomous driving (Zendel et al., 2022; Vyas et al., 2018; Lu et al., 2023) and medical diagnosis (Ren et al., 2019; Zhou et al., 2021). To solve the above problem, OOD detection (Hendrycks and Gimpel, 2016; Sun and Li, 2022; Fort et al., 2021) is proposed to accurately detect the outliers and correctly distinguish the samples from ID classes during testing.
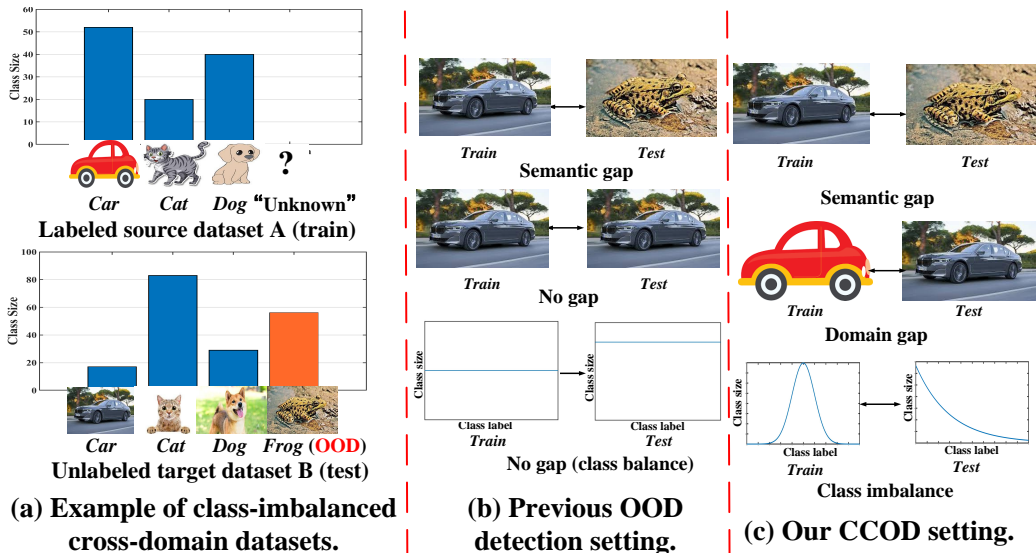
2

Figure 1: (a) Example of the class-imbalanced cross-domain out-of-distribution detection (CCOD) setting. (b) and (c) Comparison between previous models and our proposed model; previous OOD detection methods only address the semantic gap within a single domain while we aim to relieve three gaps: semantic gap (between ID samples and OOD samples), domain gap (between the labeled source domain and unlabeled target domain) and class-imbalance (between different classes).

The largest challenge for an OOD detection system is that no information about OOD samples is available during training, making it difficult to distinguish ID and OOD samples. To address the challenge, many OOD detection systems (Liang et al., 2018; Liu et al., 2020; Sun et al., 2021; Lee et al., 2018b; Mohseni et al., 2020; Vyas et al., 2018) calibrate the distribution of the softmax layer for OOD detection. Other systems (Yu and Aizawa, 2019; Zaeemzadeh et al., 2021; Hsu et al., 2020; Ming et al., 2023) aim to leverage a large number of OOD samples to learn the discrepancy between ID/OOD samples at training time, then detect the OOD samples during testing. Most OOD detection systems (Liang et al., 2018; Liu et al., 2020; Sun et al., 2021; Lee et al., 2018b; Mohseni et al., 2020; Vyas et al., 2018) have achieved remarkable performance when the training and testing sets are class-balanced and belong to the same domain. In real-world expert systems, the training set and the testing set are often from different domains since there are various difficulties collecting samples from different domains. As shown in

3

Figure 1, when we train an OOD detection system in the source dataset A, the system can extract knowledge about three ID classes (*car*, *cat* and *dog*) with the same class size in the cartoon domain. When we utilize the trained system on the target dataset B for OOD detection, the model will encounter samples from an "unknown" class (here images of *frog*, not present in the source dataset), which do not belong to the label set of the source domain, and those should be treated as OOD. As shown in Figure 1(b), the number of samples in any class is nearly the same between the source and the target dataset, *i.e., balanced classes*. Obviously, it is difficult for this assumption to hold true, since it is unrealistic that we collect all the samples from a single domain and make all classes the same size. However, domain gap and class-imbalance (Figure 1(a)) in real-world OOD detection problems will severely limit their detection ability.

To this end, in this paper we pose a more realistic yet challenging setting: class-imbalanced cross-domain OOD detection (CCOD) to handle the three gaps in Figure 1(c): the semantic gap between ID and OOD samples, the domain gap between source and target domains, and the class-imbalance between different classes. The main challenges of our CCOD task are two-fold: 1) a robust OOD detection system should both accurately detect OOD samples and correctly classify ID samples; 2) the designed OOD detection system needs to extract robust and discriminative features despite the semantic gap, domain gap, and class-imbalance. To address the aforementioned challenges, we propose a novel uncertainty-aware adaptive semantic alignment (**UASA**) network based on four novel and carefully-designed modules: a label-driven prototype building module, a prototype-guided domain alignment module, an adaptive threshold generation module and an uncertainty-aware target clustering module. In the label-driven prototype building module, we build label-driven prototypes by classifying labeled source samples, where prototypes and labels are bijectively mapped in the source domain. In the prototype-guided domain alignment module, we leverage these label-driven prototypes to conduct the target classification task. Given a set of ID classes, some OOD samples are far from all ID samples in the latent space, while others may be semantically close to certain ID classes. Thus, a specific threshold is required for each sample for OOD detection. For each target sample, we generate an adaptive OOD threshold to handle the semantic gap in the adaptive threshold generation module. Finally, we group the semantically similar target samples into a cluster in the uncertainty-aware target clustering module to reduce the negative impact of class-imbalance.

4

To this end, our main contributions are summarized as follows:

- We introduce a more practical and challenging setting for the OOD detection task called CCOD, where three gaps (semantic gap between ID samples and OOD samples, domain gap between source domain and target domain, and class-imbalance between different classes) are considered. To the best of our knowledge, this is the first attempt to handle all three gaps for OOD detection.

- For our CCOD task, we propose a novel UASA network with four modules to handle these challenging gaps. Specifically, to close the domain gap, we build label-driven prototypes in the source domain and leverage these prototypes for classification in the target domain. To handle the semantic gap for each target sample, we generate an adaptive threshold for OOD detection. As for the class-imbalance, we conduct uncertainty-aware clustering to align target samples that share similar semantics.

- Extensive experimental results on three challenging class-imbalanced benchmarks (Office-Home, VisDA-C and DomainNet) demonstrate that UASA outperforms existing state-of-the-art approaches by a large margin. In representative cases, UASA beats all compared methods by 9.06% on the DomainNet dataset.

The rest of this paper is organized as follows: Section 2 presents related work. Section 3 describes our proposed UASA network for our CCOD task. Section 4 illustrates our performance on three challenging benchmarks. Section 5 concludes this paper.

2. Related Work

Out-of-distribution detection. As a challenging expert system task, OOD detection aims to detect test samples from distributions that do not overlap with the training distribution. Previous OOD detection systems (Liang et al., 2018; Liu et al., 2020; Sun et al., 2021; Lee et al., 2018b; Mohseni et al., 2020; Vyas et al., 2018; Yu and Aizawa, 2019; Zaeemzadeh et al., 2021; Hsu et al., 2020; Ming et al., 2023) can be divided into four types: classification-based systems (Hendrycks and Gimpel, 2016; Liang et al., 2018; Lee et al., 2018c,a), density-based systems (Kirichenko et al., 2020; Serrà et al., 2019),

distance-based systems (Techapanurak et al., 2020; Lee et al., 2018b) and reconstruction-based systems (Zhou, 2022; Yang et al., 2022a). Although previous systems have achieved decent success, most of them assume that all the datasets are from the same domain and all the classes are balanced. In fact, we always collect training and testing sets from various domains, and each class has a unique number of samples. Unlike the aforementioned OOD detection systems that only address the semantic gap between ID and OOD samples, our proposed system targets to handle three challenging gaps: semantic gap between ID and OOD samples, domain gap between source and target domains and class-imbalance between different classes.

Unsupervised domain adaptation (UDA). As a significant technology in expert systems, UDA (Ganin and Lempitsky, 2015; Kang et al., 2019; Long et al., 2016; Ru et al., 2023) aims to transfer predictive systems trained on fully-labeled data from a source domain to an unlabeled target domain. The primary objective of existing UDA systems, which are predominantly classification-based, is to mitigate the domain gap between the source and target domains (Damodaran et al., 2018; Ganin and Lempitsky, 2015; Long et al., 2015, 2017; Tzeng et al., 2014). By effectively aligning the statistical distributions of the source and target domains, these systems strive to enhance the generalization capability of the model in the target domain. Furthermore, the realm of UDA has witnessed significant advancements in the domain of visual tasks, such as video action recognition (Chen et al., 2019; Choi et al., 2020; Munro and Damen, 2020) and video segmentation (Chen et al., 2020; Ullah et al., 2024; Fang et al., 2024b). UDA-based systems (Zhang et al., 2024; Liu et al., 2024; Cui et al., 2024b) have been successfully extended to these visual tasks, enabling knowledge transfer from the labeled source domain to the unlabeled target domain, thus circumventing the need for costly manual annotation in the target domain. Previous UDA-based systems only refer to the closed setting where all the test samples are ID (Zhang et al., 2020; Ainam et al., 2021; Yang et al., 2022c). Therefore, these UDA-based systems under the closed setting are not applicable to the challenging CCOD task. Unlike them, our proposed UASA can handle the CCOD task with four carefully-designed modules.

Class-imbalanced domain adaptation (CDA). The CDA task (Tan et al., 2020a; Yang et al., 2022b; Prabhu et al., 2021) is a branch of domain adaptation, which aims to carry out domain alignment on multi-domain expert systems with biased class distribution. The main challenge for the CDA task is the class-imbalance gap (Tachet des Combes et al., 2020; Tanwisuth
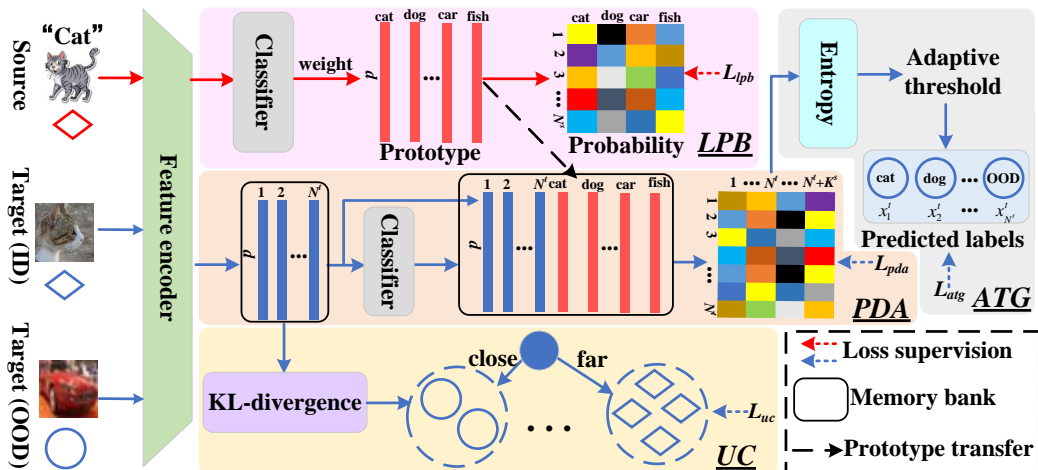
6

Figure 2: Overview of our proposed UASA system for the proposed CCOD task. Underlined module names refer to the eponymous sections in the text. First, we feed all source and target images into a ResNet-50 network (He et al., 2016) to extract their features. (i) In the label-driven prototype building (LPB) module, we build label-driven source prototypes by classifying source images. (ii) In the prototype-guided domain alignment (PDA) module, we leverage these prototypes in a memory bank for target classification. (iii) In the adaptive threshold generation (ATG) module, we automatically generate a threshold for each target sample to distinguish if the sample is OOD or ID. If it is ID, we choose the label with the highest probability as its label; otherwise, we mark it as OOD. (iv) In the uncertainty-aware target clustering (UC) module, we cluster target samples into different clusters. By aligning semantically similar samples in each cluster, we alleviate the class-imbalance gap.

et al., 2021). To relieve the class-imbalance gap, many works conduct domain adaptation on class-imbalanced datasets by exploiting the pseudo-labeled target samples (Tan et al., 2020a) or utilizing a sample selection strategy (Jiang et al., 2020). Although the above systems can close the class-imbalance gap, they focus on the ID classification task and cannot deal with the OOD detection task, which limits their applications in real-world open-set datasets. Unlike them, we can conduct ID classification in the prototype-guided domain alignment module and detect OOD samples with the adaptive threshold generation module.

3. The CCOD Task and Our Proposed UASA

Task definition for CCOD. Given a source set $D^s = \{(x_i^s, y_i^s)\}_{i=1}^{N^s}$ with N^s

samples $\{x_i^s\}_{i=1}^{N^s}$ together with associated class-labels $\{y_i^s\}_{i=1}^{N^s}$, and a target domain $D^t = \{x_j^t\}_{j=1}^{N^t}$ with N^t samples s_i^t, our posed CCOD task aims to train an OOD detection system on the combined domain $D^s \cup D^t$ to correctly classify the target samples into one of the classes shared with source domain and group OOD samples into K^t OOD classes, where $K^t \geq 1$. If the source label set is $Y^s = \{1, 2, ..., K^s\}$, the predicted target label is $Y = Y^t = \{1, ..., K^s, K^s + 1, ..., K^s + K^t\}$, where the last K^t classes are unique to the target domain, $i.e.$, OOD classes. In real-world multi-domain datasets, different classes contain various numbers of samples, $i.e.$, these classes are imbalanced. For the source and target domains, previous domain adaptation works (Turrisi et al., 2022; Nguyen et al., 2021) usually refer to the $class\text{-}balanced$ assumption, that is: $p^s(x|y = c) = p^t(x|y = c), \forall c \in Y^s$, where p^s and p^t denote the probability density functions of the source and target distributions, respectively. In our CCOD task, such a strict assumption is not imposed and each class can contain any number of samples, $i.e.$, $p^s(x|y = c) \neq p^t(x|y = c), \exists c \in Y^s$.

UASA network. To address the CCOD task, we propose a novel uncertainty-aware adaptive semantic alignment (UASA) system in Figure 2. Specifically, to close the domain gap between source and target domains, we design a prototypical network to align source and target samples with the same semantics. To handle the semantic gap between ID and OOD samples, we propose an adaptive threshold generation module to distinguish ID and OOD samples in a gradual and fine-grained manner. To relieve the class-imbalance gap between different classes in the target domain, we design an uncertainty-aware target clustering strategy to form tight clusters with semantically similar samples.

3.1. Label-Driven Prototype Building for Source Classification

To fully understand these images, the designed system is required to close the domain gap between source and target domains. Therefore, most UDA-based systems (Peng et al., 2020; Melas-Kyriazi and Manrai, 2021; Kang et al., 2019) conduct domain alignment by mapping source and target features into a shared latent space. Although the feature mapping strategy can close the domain gap to a certain extent, it has the following disadvantages: 1) It is sensitive to OOD samples. Directly utilizing source samples will limit the generalization ability of the designed model, which makes it difficult for the model to distinguish between the domain gap and the semantic gap. 2)

In a mini-batch, missing classes from the source domain will lead to inappropriate domain adaptation, and missing classes cannot contribute to domain adaptation, limiting their performance. 3) The mapping strategy is sensitive to the class size, since UDA-based systems always pay more attention to the classes with more samples and ignore the small-scale classes, which will limit the generalization ability of the designed system.

To transfer the classification knowledge from the source domain to the target domain, we aim to construct a label-driven prototype based on the labeled source images. We first utilize a ResNet-50 network (He et al., 2016) to extract the image features in the source domain. Then, a fully-connected layer with $\mathcal{L}_2$-normalization serves as the classifier, where the learnable classifier weights are denoted as $M = \{m_c\}_{c=1}^{K^s} \in \mathbb{R}^{d \times K^s}$, where m_c is the weight of the c-th class and d denotes the feature dimension. Finally, we learn the consensus representation of each class based on the weight matrix M. For any sample $x_i^s \in \mathbb{R}^d$ in the source domain and its corresponding label $y_i^s \in \mathbb{R}$, we can train the source classifier with the following cross-entropy loss:

$$\mathcal{L}_{lpb} = -\frac{1}{N^s K^s} \sum_{(x_i^s, y_i^s) \in D^s} \sum_{c=1}^{K^s} \log p^s(y_i^s = c | x_i^s, m_c) \cdot \mathbf{1}_{\{y_i^s = c\}}, \tag{1}$$

where $p^s(y_i^s = c | x_i^s, m_c)$ is the predicted probability that x_i^s is in class c, which is computed as:

$$p^s(y_i^s = c | x_i^s, m_c) = \frac{e^{(1/\sigma \cdot m_c^\top x_i^s)}}{\sum_{j=1}^{K^t} e^{(1/\sigma \cdot m_j^\top x_i^s)}}, \tag{2}$$

where the temperature parameter σ balances the concentration degree (Hinton et al., 2015). Note that m_j is class-specific, *i.e.*, each column of M corresponds to a unique class. Therefore, we treat m_j as the source prototype of the j-th class. The prototypes we utilize have four significant advantages over those in previous works (Gao et al., 2024; Belal et al., 2024; Cui et al., 2024a): 1) They are robust to OOD samples, which can effectively assist our proposed system with domain alignment. 2) Since the weights are class-specific, these prototypes can serve as the representation of each class during training. 3) Some real-world expert systems deal with highly private data. Previous systems (Fang et al., 2024a; Sun et al., 2025; Xie et al., 2024) needed to access all the data to build their prototypes, however, our prototypes allow our system to conduct domain adaptation without accessing

the source dataset, which preserves data privacy in the source domain. 4) We build the prototypes without introducing additional parameters, which significantly reduces the computational cost to obtain the prototypes.

3.2. Prototype-Guided Domain Alignment for Target Classification

To transfer knowledge from the labeled source domain to the unlabeled target domain, previous UDA-based systems (Nguyen et al., 2022; Sicilia et al., 2022; Ren et al., 2024) mitigate the domain gap between the source and target domains in an adversarial way. However, the real-world setting is more challenging due to the semantic gap (between ID and OOD samples) and imbalanced classes. Therefore, forceful domain alignment between the source domain and the target domain might lead to catastrophic misalignment. To this end, we design a prototype-guided domain alignment module for target classification. To correctly align semantically similar samples, we feed all $\mathcal{L}_2$-normalized target features into a memory bank $Z = [z_1, z_2, ..., z_{N^t}] \in \mathbb{R}^{d \times N^t}$. Then, we concatenate the memory bank Z and the source classification weight M to obtain the cross-domain representation $F = [Z, M] = [z_1, ..., z_{N^t}, m_1, ..., m_{K^s}]$, where $[\cdot, \cdot]$ denotes the concatenation operation. During each iteration, we update the target features in the memory bank Z. Therefore, we use the memory bank to conduct domain alignment with the following loss:

$$\mathcal{L}_{pda} = -\frac{1}{|\mathcal{B}^t|(N^t + K^s)} \sum_{i \in \mathcal{B}^t} \sum_{j=1, j \neq i}^{N^t + K^s} p_{ij}^t \log(p_{ij}^t), \tag{3}$$

where $p_{ij}^t = e^{(1/\sigma \cdot f_j^\top x_i^t)} / \sum_{l=1, l \neq i}^{N^t + K^s} e^{(1/\sigma \cdot f_l^\top x_i^t)}$ denotes the probability that the target sample i belongs to label y_j; $\mathcal{B}^t$ is the corresponding mini-batch of each target domain mini-batch; and f_j and f_l are the j-th and l-th columns of F, respectively. We can minimize the entropy of the similarity between the target samples and source prototypes under Equation (3), which aligns each target sample to a source prototype or its paired neighbor in a mini-batch. Therefore, these target ID samples will be classified into the correct classes.

3.3. Adaptive Threshold Generation for Target OOD Detection

The main challenge of our CCOD task is correctly detecting OOD samples in the target domain. In real-world systems, the relationship between ID and OOD samples varies significantly. For example, some OOD samples are

far from all ID samples in the latent space and are easy to recognize as OOD samples. For convenience, we refer to these OOD samples as "easy OOD samples". On the contrary, some OOD samples may be semantically close to certain ID classes, and we call them "hard OOD samples" as they are hard to distinguish as OOD samples. During inference, OOD detection systems tend to overconfidently predict the results for those hard OOD samples as similar to ID classes, which corresponds to a small threshold for the similarity to ID samples. Also, some classes may contain more easy OOD samples, where we need a larger threshold to avoid OOD samples being misclassified as ID classes. Considering that easy OOD samples have higher entropy, a higher threshold can help us detect these OOD samples and obtain better performance. We observe that in most OOD detection systems, ID samples always have lower entropy than OOD samples (Li and Vasconcelos, 2020; Sun and Wang, 2022; Vernekar et al., 2019), which is an essential criterion to distinguish ID and OOD samples. Previous OOD detection systems predefine a fixed entropy threshold o' for all the samples to assess whether any target sample x_i^t is OOD or not. If the entropy of x_i^t is greater than o', x_i^t is OOD, and vice versa. In fact, on real-word datasets we need different thresholds to handle various scenarios. The fixed threshold makes previous OOD detection systems sensitive to parameter tuning and weakens their robustness in complex scenarios. Therefore, we design a novel adaptive threshold generation policy to learn an adaptive threshold for each target sample.

To adaptively generate sample-wise thresholds in the target domain, we generate a pseudo-label for each target sample in a self-supervised manner. For convenience, H_i denotes the set of target samples that are labeled as class i. Initially, we do not distinguish OOD samples, $i.e.$, $H_1 \cup ... \cup H_{K^s} = \{1, ..., N^t\}$. Since the easy OOD samples often have larger entropy than the hard OOD samples, we calculate the mean entropy of each class to recognize which class consists of more easy OOD samples. We denote the softmax output of the classifier as p^t, where p_i^t denotes the i-th target sample's probability distribution. Thus, its corresponding class-wise entropy T_i is given by:

$$T_i = \frac{1}{|H_i|} \sum_{j=1}^{|H_i|} Q(p_{H_{ij}}^t), \tag{4}$$

11

where $i \in Y^t$; and $Q(\cdot)$ is the sample-wise entropy function. We set the threshold o_i of the target sample x_i^t using its entropy T_i by:

$$o_i = \frac{\alpha(T_i - \min(T) - \max(T))}{\max(T) - \min(T)} \log K^s, \tag{5}$$

where α is an adjustable hyperparameter. Based on the sample-wise threshold o_i, we classify ID samples and detect OOD samples. Thus, for the target sample x_i^t, its predicted label is:

$$\bar{y}_i^t = \begin{cases} \arg\max_j p_{ij}^t, & Q(p_i^t) \leq o_{\arg\max_j p_{ij}^t}, \\ OOD, & \text{otherwise}, \end{cases} \tag{6}$$

where the adaptive threshold $o_{\arg\max_j p_{ij}^t}$ will be different for individual target samples. If entropy $Q(p_i^t)$ is not higher than the adaptive threshold, x_i^t is ID and we predict its label as $\arg\max_j p_{ij}^t$. Otherwise, x_i^t is OOD. To obtain a clearer ID/OOD decision boundary, we utilize the following entropy separation loss:

$$\mathcal{L}_{atg} = -\frac{1}{|\mathcal{B}^t|} \sum_{i \in \mathcal{B}^t} \mathcal{L}_{atg}(p_i^t),$$

$$\mathcal{L}_{atg}(p_i^t) = \begin{cases} 0, & ||o_i' - Q(p_i^t)||_2^2 < \Delta, \\ ||o_i' - Q(p_i^t)||_2^2, & \text{otherwise}, \end{cases} \tag{7}$$

where $|| \cdot ||_2$ denotes the $\mathcal{L}_2$ norm, $o_i' = o_{\arg\max_j p_{ij}^t}$, and Δ is the confidence interval. The confidence interval Δ allows us enable the entropy separation loss to keep target samples from the ID/OOD decision boundary.

3.4. Uncertainty-Aware Target Clustering for Class-Imbalance

To close the class-imbalance gap, we design a novel uncertainty-aware clustering module for the target domain. During clustering, we first align the target samples with their corresponding cluster centers by conducting clustering (*e.g.*, K-means clustering) and then tightening the clusters. In a target domain mini-batch $\mathcal{B}^t$, we denote any two samples as x_i^t and x_j^t, and their corresponding probability distributions as p_i^t and p_j^t, respectively. If x_i^t

and x_j^t share the same predicted label, we should align them. For supervision, we introduce the Kullback Leibler divergence loss (KL loss):

$$\mathcal{L}_{kl}(p_i^t, p_j^t) = \frac{1}{2}[\mathcal{F}_{kl}(p_i^t|p_j^t) + \mathcal{F}_{kl}(p_j^t|p_i^t)], \tag{8}$$

where $\mathcal{F}_{kl}(\cdot|\cdot)$ denotes the KL divergence function between two samples. Since real-world OOD samples are often semantically different, directly minimizing the distance between them will confuse the OOD detector, resulting in inaccurate OOD detection results. To only align semantically samples, we feed all $\mathcal{L}_2$-normalized target features into a memory bank $Z = [z_1, z_2, ..., z_{N^t}] \in \mathbb{R}^{d \times N^t}$. During each epoch, we update the target features in the memory bank Z. Then, we conduct uncertainty-aware target clustering on the memory bank Z to obtain A clusters, where $C \in \mathbb{R}^{d \times A}$ denotes these clusters and $A > K^s$. We can obtain the corresponding cluster index for each target sample x_j^t as follows:

$$a_j = \arg\max_i \cos(c_i, x_j^t), \tag{9}$$

where $\cos(\cdot, \cdot)$ denotes the cosine similarity function, and c_i is the i-th column of C, which can be treated as the center of the i-th cluster. Based on the clustering strategy, semantically different samples will be allocated to different clusters. For convenience, we define the set of pseudo-labels as $\{1, \cdots, K^s, \cdots, A\}$.

Incorrect pseudo-labels may lead to unsatisfactory OOD detection performance if we directly utilize these labels in the KL loss. To relieve the negative effect of incorrect pseudo-labels, we define any two samples (x_i^t and x_j^t) in the same mini-batch as a pair $\{x_i^t, x_j^t\}$. Therefore, we should assign different weights to different pairs. In particular, we will assign higher weights to the pairs with higher confidence scores, and vice versa. If a target sample is labeled as an ID sample in Section 3.3, we use the largest logit of its probability distribution across ID classes as its confidence score. For an OOD sample, we define its confidence score as the entropy of its probability distribution. In the mini-batch, we define the weight m_{ij} of each pair $\{x_i^t, x_j^t\}$ as:

$$m_{ij} = \begin{cases} 0, & \bar{y}_i^t \neq \bar{y}_j^t, \\ \frac{s_i + s_j}{2}, & \text{otherwise}, \end{cases} \tag{10}$$

where s_i and s_j are confidence score of target samples i and j, respectively.

13

Therefore, we introduce the following loss to conduct uncertainty-aware target clustering:

$$\mathcal{L}_{uc} = \frac{1}{|\mathcal{B}^t|} \sum_{i \in \mathcal{B}^t, j \in \mathcal{B}^t, i \neq j} m_{ij} \cdot \mathcal{L}_{kl}(p_i^t, p_j^t). \tag{11}$$

In Equation (11) we make semantically similar samples (*i.e.*, samples that share the same pseudo-label) tighter, which will improve the robustness of our system under the class-imbalance gap.

Overall, our total loss is formulated as follows:

$$\mathcal{L} = \mathcal{L}_{lpb} + \lambda_1 \mathcal{L}_{pda} + \lambda_2 \mathcal{L}_{atg} + \lambda_3 \mathcal{L}_{uc}, \tag{12}$$

where λ_1, λ_2 and λ_3 are hyperparameters that balance the importance of the different losses.

4. Experiments and Analysis

Datasets. To evaluate the performance of our proposed system, we need multi-domain datasets. Following (Saito and Saenko, 2021a), we utilize three popular yet challenging datasets: DomainNet (Peng et al., 2019), Office-Home (Venkateswara et al., 2017a) and VisDA-C (Peng et al., 2018; Li et al., 2021).

1) DomainNet (Peng et al., 2019; Tan et al., 2020b) contains 600k images from 345 classes on 4 widely used domains: real (**R**), clipart (**C**), painting (**P**) and sketch (**S**). All 345 classes are present in each domain. We choose a domain as the labeled source domain and the remaining three domains as unlabeled target domains. By treating one domain as the source domain and another domain as the target domain, we can construct a transfer task from the source domain to the target domain. Considering all the domains, we track the following transfer tasks: R→C, R→S, R→P, C→R, C→S, C→P, S→R, S→C, S→P, P→C, P→S, P→R. In each source domain, we regard the first 45 classes in alphabetical order as the source domain input, and drop the remaining (300 classes). In each target domain, we utilize all 345 classes as the target domain input. For example, in the R→C task, we use the first 45 classes in the R domain as the source domain input, and all 345 classes (the first 45 classes are ID and the last 300 classes are OOD) in the C domain as the target domain input.

2) Office-Home (Venkateswara et al., 2017b) contains 15,500 images from 65 classes on 4 domains: art (AR), clipart (CL), product (PR) and real-world

(RE). Due to the page limitation, we only utilize 3 domains: CL, PR and RE. Similarly, we select one domain as the labeled source domain and the remaining two domains as unlabeled target domains. We consider 6 transfer tasks: RE→PR, RE→CL, PR→RE, PR→CL, CL→RE and CL→PR. We choose the first 50 classes in alphabetical order as each source domain's input. In the target domain, all the classes (50 ID classes and 15 OOD classes) are used as input.

3) Following (Li et al., 2021), we utilize the class-imbalanced version of VisDA-C (Peng et al., 2018; Li et al., 2021) for our CCOD task. VisDA-C contains 280,157 images from 12 classes on 3 domains. Similarly, we select a labeled source domain and treat the remaining two domains as unlabeled target domains. We denote the class size of the i-th class as O_i. For convenience, we define $N_{\max} = \max\{O_1, O_2, ..., O_{12}\}$ and $N_{\min} = \min\{O_1, O_2, ..., O_{12}\}$ An imbalance factor μ is used to indicate the degree of class-imbalance, which is defined by $\mu = N_{\max}/N_{\min}$.

Implementation details. For a fair comparison, we follow (Saito et al., 2020) and use a ResNet-50 network (He et al., 2016) as the feature encoder. We replace the last layer of the ResNet-50 network with the new weight matrix to obtain the weight of each class during classification. For all the datasets, we set $\sigma = 0.05$ in Equation (2), $\Delta = 0.5$ in Equation (7), $\alpha = 0.15$ in Equation (5), and $A = 2.5K^s$. In Equation (12), we set $\lambda_1 = 0.05$, $\lambda_2 = 0.1$, $\lambda_3 = 0.1$. We set the mini-batch size $|\mathcal{B}^t|$ as 128 on VisDA-C, and 32 on Office-Home and DomainNet. Similarly, the learning rate is set at 1×10^{-2} on Office-Home and DomainNet, and 2×10^{-2} on VisDA-C . The stochastic gradient descent optimizer with a momentum of 0.9 is utilized for model optimization. We implement our proposed method in PyTorch (Paszke et al., 2019). Our codes are available in Github.

Evaluation metrics. We follow (Bucci et al., 2020) to adopt the **HOS** score for evaluation. **HOS** is defined as the harmonic mean between **OS*** and **UNK** metrics:

$$HOS = 2 \times \mathbf{OS}^* \times \mathbf{UNK}/(\mathbf{OS}^* + \mathbf{UNK}), \tag{13}$$

where **OS*** denotes the average accuracy over the ID classes only and **UNK** is the recall metric that denotes the ratio of the number of correctly predicted OOD samples over the total number of OOD samples in the target dataset. Since **HOS** score considers ID classification and OOD detection simultaneously, we use it as the evaluation metric for CCOD; it is the most

Table 1: Performance comparison with state-of-the-art methods for CCOD on the DomainNet dataset.

Models	R→C	R→S	R→P	C→R	C→S	C→P	S→R	S→C	S→P	P→C	P→S	P→R	Mean
MSP	28.75	30.14	28.76	10.03	24.11	21.76	12.93	19.54	20.17	14.26	10.76	11.29	19.38
ODIN	32.96	33.78	35.82	16.92	23.70	20.53	18.23	16.75	23.14	13.92	16.75	10.33	21.90
UAN	45.21	50.85	52.30	20.53	32.62	36.81	26.15	19.03	29.14	23.28	15.69	9.43	30.09
Energy	46.72	44.59	51.93	38.46	35.72	34.16	24.83	22.69	31.72	28.94	24.83	49.52	36.18
CMU	49.12	48.17	52.58	51.36	42.89	40.43	52.13	47.80	48.35	43.86	46.73	48.57	47.67
CIDER	50.96	50.37	54.82	48.99	47.32	51.94	55.36	40.83	51.42	44.17	48.32	51.96	49.71
ROS	54.17	52.03	56.49	71.24	56.50	59.31	70.52	52.28	60.74	45.59	50.97	57.86	57.31
STA	57.53	57.48	61.02	62.19	59.96	57.25	69.04	59.02	62.83	52.33	52.01	51.65	58.53
DANCE	60.28	59.93	65.86	70.82	58.53	60.32	73.77	62.40	68.19	56.31	59.17	64.28	63.32
OSBP	61.35	61.04	67.19	72.63	53.75	54.33	73.05	54.44	67.23	53.14	59.42	66.20	61.98
Ovanet	64.01	63.43	67.65	71.13	61.42	65.43	70.36	66.75	72.38	62.19	63.94	68.25	66.41
UASA	**68.53**	**65.12**	**69.90**	**77.82**	**62.88**	**65.52**	**83.46**	**68.51**	**73.05**	**63.23**	**65.18**	**77.31**	**70.04**

Table 2: Performance comparison with state-of-the-art methods for CCOD on the Office-Home dataset.

Models	RE→PR	RE→CL	PR→RE	PR→CL	CL→RE	CL→PR	Mean
UAN	14.82	6.13	9.52	3.82	6.17	8.32	8.13
MSP	18.62	12.35	11.17	6.28	10.37	12.84	11.94
ODIN	22.31	18.30	10.72	8.13	11.55	14.72	14.29
ROS	50.26	44.12	54.62	42.87	43.50	35.72	45.18
CIDER	50.49	42.13	50.26	40.38	39.75	34.33	42.89
Energy	51.37	40.19	52.75	38.26	44.23	37.52	44.05
CMU	53.04	39.82	50.76	35.10	41.35	36.29	42.73
OSBP	60.34	49.12	63.27	46.20	56.37	57.43	55.46
STA	61.23	48.01	64.72	48.96	54.62	55.34	55.48
DANCE	61.27	50.93	63.18	53.96	60.15	59.03	58.09
Ovanet	63.21	49.02	67.72	46.23	62.07	57.48	57.62
UASA	**67.48**	**52.53**	**67.85**	**55.29**	**62.59**	**61.08**	**61.14**

Table 3: Performance comparison with state-of-the-art methods for CCOD on the VisDA-C dataset.

Models	$\mu = 100$, $K^s = 9$	$\mu = 50$, $K^s = 9$	$\mu = 10$, $K^s = 9$	$\mu = 5$, $K^s = 9$	$\mu = 100$, $K^s = 10$	$\mu = 50$, $K^s = 10$	$\mu = 10$, $K^s = 10$	$\mu = 5$, $K^s = 10$	Mean
ODIN	18.52	27.34	28.17	28.40	29.43	37.92	34.95	35.72	30.06
CMU	23.58	25.31	29.04	29.18	29.82	39.37	33.86	35.29	30.68
MSP	25.32	22.18	20.16	20.87	27.92	36.83	30.24	33.42	27.12
Energy	32.19	29.43	23.75	23.52	20.34	26.17	23.59	24.96	25.50
OSBP	42.85	43.62	43.95	44.03	45.38	48.12	46.73	45.72	45.05
STA	43.08	43.62	45.37	45.78	42.14	40.13	41.09	41.27	42.81
CIDER	44.18	42.56	43.82	43.26	40.29	41.13	42.40	41.35	42.37
ROS	45.12	44.93	49.55	50.03	45.27	40.86	44.38	44.79	45.62
Ovanet	46.40	48.73	51.08	50.84	47.13	49.41	47.28	48.33	48.65
DANCE	50.13	44.09	48.70	48.62	41.68	39.67	39.55	40.18	44.08
UAN	50.21	51.14	48.32	49.36	43.07	44.18	43.86	43.72	46.73
UASA	**54.11**	**54.96**	**54.07**	**54.29**	**48.03**	**52.16**	**50.13**	**51.34**	**52.39**

Table 4: Performance comparison for the CCOD task on the Office-Home dataset based on Saito et al.'s settings(Saito and Saenko, 2021b; Saito et al., 2020).

Models	RE→PR	RE→CL	PR→RE	PR→CL	CL→RE	CL→PR	Mean
STA	53.45	45.14	47.12	41.27	43.68	43.72	45.73
OSBP	46.52	41.41	45.68	40.43	46.26	45.14	44.24
Ovanet	60.30	51.69	58.43	44.61	70.64	63.12	58.13
Dance	73.75	59.42	78.06	59.08	77.63	67.05	69.17
UASA	**80.82**	**64.53**	**83.58**	**63.15**	**81.26**	**72.84**	**74.36**

important metric in our CCOD task. To obtain a statistical analysis of the experimental results, we also report the average HOS score of different transfer tasks.

Compared methods. For better reproducibility, we re-implement several state-of-the-art open-source methods: MSP (Hendrycks and Gimpel, 2017), ODIN (Liang et al., 2018), OSBP (Saito et al., 2018), STA (Liu et al., 2019), ROS (Bucci et al., 2020), UAN (You et al., 2019), CMU (Fu et al., 2020),

DANCE (Saito et al., 2020), Energy (Liu et al., 2020), Ovanet (Saito and Saenko, 2021b), and CIDER (Ming et al., 2023). Since Energy (Liu et al., 2020) is easy to implement and performs well, we treat it as a baseline for the CCOD task. Based on the official code and settings, we implement all the methods on all three datasets.

4.1. Class-Imbalanced Cross-Domain OOD Detection

As shown in Tables 1-3, our proposed UASA outperforms all compared methods with a large margin for each transfer task, showing the effectiveness of UASA. Particularly, on the DomainNet dataset, UASA beats the compared methods by 9.06% for the P→R task in Table 1. The main reason is that the DomainNet dataset contains many classes, and there is little difference between different classes. These small differences make it difficult for the previous methods to distinguish ID and OOD samples. However, our UASA can generate adaptive thresholds for OOD detection to handle small differences between ID and OOD samples. For the Office-Home dataset, UASA improves the performance by 4.27% for the RE→PR task in Table 2 because the types of different domains on the Office-Home dataset vary significantly. The main challenge is aligning various domains. Our proposed UASA can effectively build label-driven prototypes in the source domain, and then conduct domain alignment based on prototypes. As for the VisDA-C dataset, UASA achieves 3.90% improvement when $\mu = 100, C = 9$ in Table 3. The significant improvement is because our UASA can cluster semantically similar samples to eliminate the negative impact of imbalanced classes.

4.2. Class-Balanced Cross-Domain OOD Detection

To comprehensively analyze our model's performance, we compare UASA with some representative state-of-the-art methods under the class-balanced setting. Table 4 reports the corresponding results. UASA still obtains better performance than these compared methods for all the domain transfer tasks, especially in the RE→PR task, where UASA outperforms compared methods by 7.07%. Since the class-balanced setting is easier than the class-imbalanced setting, all methods perform better. UASA still achieves the best performance due to the label-driven prototype and adaptive threshold that handle the domain gap and semantic gap.

Feature visualization. We randomly choose 40 "cat" source samples and 60 target samples to investigate the feature domain distributions in each
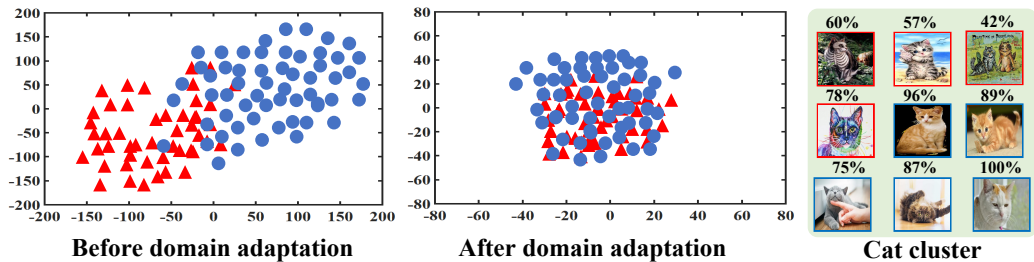
Before domain adaptation   **After domain adaptation**   **Cat cluster**

Figure 3: Visualizations for the P→R task on DomainNet. Left and Middle: T-SNE visualizations of "before domain adaptation" (Left) and "after domain adaptation" (Middle), where red triangles denote source "cat" samples and blue circles denote target "cat" samples. Right: Visualization of our clustering results. We show partial samples from the "Cat" cluster, where the labeled percentage is larger than 85%. We report the probability above each image. Images with red edges are from the painting domain. Images with blue edges are from the real-world domain.
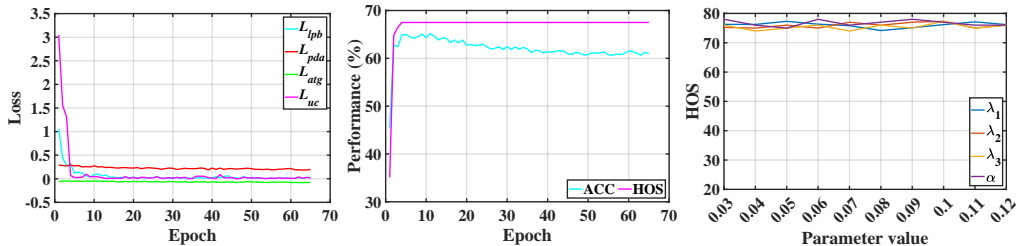

Figure 4: Left and Middle: ablative CCOD performance in terms of loss (Left) and performance (Middle) for the P→R task on the DomainNet dataset across training epochs, where "ACC" means "source classification accuracy". Right: Parameter sensitivity $(\lambda_1, \lambda_2, \lambda_3, \alpha)$.

domain for the P→R task on DomainNet. Figure 3 shows the t-SNE visualizations (Van der Maaten and Hinton, 2008) of "before domain adaptation" and "after domain adaptation" in our UASA. Obviously, there is a large distribution gap between the source and target domains, and UASA can effectively close the domain gap with label-driven prototypes.

Qualitative analysis. To qualitatively investigate the effectiveness of UASA, we report some representative examples on DomainNet in Figure 3. The visualization results show that UASA can close the domain gap with high confidence.

Training process. We analyze the training process and performance in Figure 4. We obtain some representative observations: (i) During training, as the

19

Table 5: Main ablation study on the VisDA-C dataset, where "PDA" means "prototype-guided domain alignment module", "UC" means "uncertainty-aware target clustering module", and "ATG" means "adaptive threshold generation module".

Models	$\mu = 100,$ $K^s = 9$	$\mu = 50,$ $K^s = 9$	$\mu = 10,$ $K^s = 9$	$\mu = 5,$ $K^s = 9$	$\mu = 100,$ $K^s = 10$	$\mu = 50,$ $K^s = 10$	$\mu = 10,$ $K^s = 10$	$\mu = 5,$ $K^s = 10$
w/o PDA	47.56	48.13	48.25	42.39	48.56	46.03	45.33	45.86
w/o UC	48.25	50.22	48.53	49.32	42.94	46.87	46.72	47.40
w/o ATG	48.32	49.40	49.58	50.34	41.26	48.24	47.01	47.69
Full	**54.11**	**54.96**	**54.07**	**54.29**	**48.03**	**52.16**	**50.13**	**51.34**

epoch number increases, all the losses ($\mathcal{L}_{lpb}$, $\mathcal{L}_{pda}$, $\mathcal{L}_{atg}$ and $\mathcal{L}_{uc}$) decrease, and the performance (ACC and HOS) increases, illustrating that UASA can both classify source samples and detect target OOD samples simultaneously. (ii) Our full UASA converges quickly and with satisfactory performance within 50 epochs. The main reason is that each designed model mostly contains easy computations with low complexity, *e.g.*, the index operation in Equation (1). In Section 3.1, we utilize the class weight m_j as the source prototype of the j-th class, which also reduces computational cost. Therefore, our full model has low computational complexity and is more efficient with respect to execution time on the challenging CCOD task.

Parameter sensitivity. Additionally, we investigate the robustness of the proposed model to different hyper-parameters ($\lambda_1, \lambda_2, \lambda_3, \alpha$) for the P→R task on the DomainNet dataset. As shown in Figure 4, within a wide range of these hyper-parameters the performance only varies slightly, indicating robustness to different choices of these parameters. For convenience, we choose $\lambda_1 = 0.05$, $\lambda_2 = 0.1$, $\lambda_3 = 0.1$, and $\alpha = 0.15$.

4.3. Ablation Study

Main ablation study. To evaluate the effectiveness of each module in our UASA, we conduct the main ablation study on the VisDA-C dataset. The corresponding experimental results are in Table 5. We find that each module significantly contributes to the final performance, illustrating that the three modules can effectively reduce all three gaps in the CCOD setting (semantic gap, domain gap and class-imbalance). Moreover, the prototype-guided distribution alignment module achieves the largest improvement, demonstrating

Table 6: Effect of the prototype-guided domain alignment module on the VisDA-C dataset.

Variant	$\mu = 100, K^s = 9$	$\mu = 50, K^s = 9$	$\mu = 10, K^s = 9$	$\mu = 5, K^s = 9$	$\mu = 100, K^s = 10$	$\mu = 50, K^s = 10$	$\mu = 10, K^s = 10$	$\mu = 5, K^s = 10$
KL loss	52.45	50.72	53.48	54.05	**48.10**	51.59	**50.42**	50.87
Ours	**54.11**	**54.96**	**54.07**	**54.29**	48.03	**52.16**	50.13	**51.34**
$\sigma = 0.8$	53.55	54.71	53.20	54.18	47.85	51.76	49.88	51.03
$\sigma = 0.9$	53.72	54.80	53.88	54.04	47.59	51.82	50.02	51.19
$\sigma = 1.0$	**54.11**	**54.96**	**54.07**	**54.29**	**48.03**	**52.16**	**50.13**	**51.34**
$\sigma = 1.1$	53.94	54.81	53.60	54.15	47.59	51.80	49.86	51.17
$\sigma = 1.2$	53.80	54.66	53.29	54.21	47.84	51.38	49.74	50.92

that it can effectively transfer these label-driven prototypes from the labeled source domain to these unlabeled target domains for OOD detection. In addition, the distribution alignment module bridges the distribution gap between source and target domains.

Analysis of the prototype-guided domain alignment module. To evaluate the ability to close the domain gap, we conduct an ablation study on the prototype-guided domain alignment module in Table 6, where "KL loss" means that we replace the cross-entropy loss in Table 3 with KL loss. Our cross-entropy loss outperforms KL loss in most cases. Also, we test different values of σ and achieve the best performance when $\sigma = 1.0$.

Effect of adaptive threshold generation module. The adaptive threshold generation module is the core component that directly affects the OOD detection results. To investigate its effectiveness, we implement different variants of the adaptive threshold generation module in Table 7, where "Fixed threshold" indicates that we set each threshold q_i to a constant (we set $q_i = \log(K^s)/2$) and "Adaptive threshold" refers to our full adaptive threshold generation module. In the $\mathcal{L}_{atg}(p_i)$, we introduce the parameter Δ. Table 7 explores a range of values for Δ with the best performance when $\Delta = 0.5$.

Influence of the uncertainty-aware clustering module. We also analyze the influence of our uncertainty-aware clustering module in Table 8. For Equation (8), we compare the KL loss and cross-entropy loss. We find that the KL loss addresses the class-imbalance better than the cross-entropy loss. In addition, we test different cluster numbers to find the best cluster number

Table 7: Effect of the adaptive threshold generation module on the VisDA-C dataset.

Variant	$\mu = 100,$ $K^s = 9$	$\mu = 50,$ $K^s = 9$	$\mu = 10,$ $K^s = 9$	$\mu = 5,$ $K^s = 9$	$\mu = 100,$ $K^s = 10$	$\mu = 50,$ $K^s = 10$	$\mu = 10,$ $K^s = 10$	$\mu = 5,$ $K^s = 10$
Fixed	51.32	50.87	51.69	52.14	47.21	51.08	48.75	49.72
Adaptive	**54.11**	**54.96**	**54.07**	**54.29**	**48.03**	**52.16**	**50.13**	**51.34**
$\Delta = 0.3$	53.38	53.75	53.50	53.91	47.95	51.87	49.85	50.40
$\Delta = 0.4$	53.62	54.13	53.76	53.92	47.81	52.04	50.04	50.83
$\Delta = 0.5$	**54.11**	**54.96**	**54.07**	**54.29**	**48.03**	**52.16**	**50.13**	**51.34**
$\Delta = 0.6$	54.07	52.19	53.88	54.02	47.92	51.98	49.85	50.27
$\Delta = 0.7$	53.75	53.68	53.59	53.77	47.94	51.83	49.70	50.03

Table 8: Effect of the uncertainty-aware target clustering module on the VisDA-C dataset.

Variant	$\mu = 100,$ $K^s = 9$	$\mu = 50,$ $K^s = 9$	$\mu = 10,$ $K^s = 9$	$\mu = 5,$ $K^s = 9$	$\mu = 100,$ $K^s = 10$	$\mu = 50,$ $K^s = 10$	$\mu = 10,$ $K^s = 10$	$\mu = 5,$ $K^s = 10$
CE loss	53.24	52.19	53.88	54 06	47.27	51.89	48.50	49.11
Ours	**54.11**	**54.96**	**54.07**	**54.29**	**48.03**	**52.16**	**50.13**	**51.34**
$A = 2.4K^s$	53.85	54.22	53.64	53.97	47.53	51.45	49.83	50.90
$A = 2.4K^s$	53.98	54.15	53.26	54.08	47.82	51.60	49.92	50.80
$A = 2.5K^s$	**54.11**	**54.96**	**54.07**	**54.29**	48.03	**52.16**	**50.13**	**51.34**
$A = 2.6K^s$	53.48	53.95	53.81	53.97	**48.21**	51.84	49.88	51.10
$A = 2.7K^s$	53.30	53.88	54.01	53.65	47.35	51.66	49.75	50.88

A. From Table 8, we can achieve the best performance when $A = 2.5K^s$.
Impact of different loss functions. In our proposed UASA, we introduce different losses to supervise different modules. We remove individual losses in Table 9 and observe that we achieve the best performance when we utilize all the losses for model training. It demonstrates that each loss is effective in our proposed UASA during training.

Table 9:   Effect of different losses on the VisDA-C dataset.

Variant	$\mu = 100$, $K^s = 9$	$\mu = 50$, $K^s = 9$	$\mu = 10$, $K^s = 9$	$\mu = 5$, $K^s = 9$	$\mu = 100$, $K^s = 10$	$\mu = 50$, $K^s = 10$	$\mu = 10$, $K^s = 10$	$\mu = 5$, $K^s = 10$
w/o $\mathcal{L}_{lpb}$	51.08	52.89	51.90	52.37	47.82	51.88	48.65	50.10
w/o $\mathcal{L}_{pda}$	51.85	52.76	52.44	51.98	46.23	51.50	48.72	49.59
w/o $\mathcal{L}_{atg}$	52.10	53.08	52.95	52.87	47.18	50.80	49.24	50.28
w/o $\mathcal{L}_{uc}$	52.36	53.67	53.15	53.28	47.70	51.22	49.08	50.84
Full	**54.11**	**54.96**	**54.07**	**54.29**	**48.03**	**52.16**	**50.13**	**51.34**

5. Conclusion

In this paper, we pose a novel yet challenging setting for an OOD detection system: CCOD, where we consider three gaps: the semantic gap between ID and OOD classes, the domain gap between source and target domains, and the class-imbalance between different classes. To tackle this challenging setting, we propose a novel uncertainty-aware adaptive semantic alignment (UASA) network to handle all three gaps. Experimental results on three challenging datasets show the effectiveness of UASA. In representative cases, UASA outperforms all compared methods by 9.06% on the DomainNet dataset. In the future, we will extend our proposed UASA system to more complex video datasets to further improve its generalization ability. We also aim to explore different ways to align source/target domains to improve the model.

6. Acknowledgement

References

Ainam, J.P., Qin, K., Owusu, J.W., Lu, G., 2021. Unsupervised domain adaptation for person re-identification with iterative soft clustering. Knowledge-Based Systems 212, 106644.

Atmakuru, A., Chakraborty, S., Faust, O., Salvi, M., Barua, P.D., Molinari, F., Acharya, U., Homaira, N., 2024. Deep learning in radiology for lung cancer diagnostics: A systematic review of classification, segmentation, and predictive modeling techniques. Expert Systems with Applications , 124665.

Belal, A., Meethal, A., Romero, F.P., Pedersoli, M., Granger, E., 2024. Multi-source domain adaptation for object detection with prototype-based mean teacher, in: Proceedings of the IEEE/CVF Winter Conference on Applications of Computer Vision, pp. 1277–1286.

Bucci, S., Loghmani, M.R., Tommasi, T., 2020. On the effectiveness of image rotation for open set domain adaptation, in: European Conference on Computer Vision, Springer. pp. 422–438.

Chen, M.H., Kira, Z., AlRegib, G., Yoo, J., Chen, R., Zheng, J., 2019. Temporal attentive alignment for large-scale video domain adaptation, in: Proceedings of the IEEE/CVF International Conference on Computer Vision, pp. 6321–6330.

Chen, M.H., Li, B., Bao, Y., AlRegib, G., Kira, Z., 2020. Action segmentation with joint self-supervised temporal domain adaptation, in: Proceedings of the IEEE/CVF Conference on Computer Vision and Pattern Recognition, pp. 9454–9463.

Cho, W., Choo, J., 2022. Towards accurate open-set recognition via background-class regularization, in: European Conference on Computer Vision, Springer. pp. 658–674.

Choi, J., Sharma, G., Schulter, S., Huang, J.B., 2020. Shuffle and attend: Video domain adaptation, in: Computer Vision–ECCV 2020: 16th European Conference, Glasgow, UK, August 23–28, 2020, Proceedings, Part XII 16, Springer. pp. 678–695.

Tachet des Combes, R., Zhao, H., Wang, Y.X., Gordon, G.J., 2020. Domain adaptation with conditional distribution matching and generalized label shift. Advances in Neural Information Processing Systems 33, 19276–19289.

Cui, H., Zhao, L., Li, F., Zhu, L., Han, X., Li, J., 2024a. Effective comparative prototype hashing for unsupervised domain adaptation, in: Proceedings of the AAAI Conference on Artificial Intelligence, pp. 8329–8337.

Cui, X., Wang, B., Jiang, S., Liu, Z., Xu, H., Cui, L., Li, S., 2024b. Unified bi-encoder bispace-discriminator disentanglement for cross-domain echocardiography segmentation. Knowledge-Based Systems 303, 112394.

Damodaran, B.B., Kellenberger, B., Flamary, R., Tuia, D., Courty, N., 2018. Deepjdot: Deep joint distribution optimal transport for unsupervised domain adaptation, in: Proceedings of the European conference on computer vision (ECCV), pp. 447–463.

De, K., Pedersen, M., 2021. Impact of colour on robustness of deep neural networks, in: Proceedings of the IEEE/CVF international conference on computer vision, pp. 21–30.

Du, R., Chang, D., Bhunia, A.K., Xie, J., Ma, Z., Song, Y.Z., Guo, J., 2020. Fine-grained visual classification via progressive multi-granularity training of jigsaw patches, in: European Conference on Computer Vision, Springer. pp. 153–168.

Fang, Y., Chen, C., Zhang, W., Wu, J., Zhang, Z., Xie, S., 2024a. Prototype learning for adversarial domain adaptation. Pattern Recognition , 110653.

Fang, Y., Yap, P.T., Lin, W., Zhu, H., Liu, M., 2024b. Source-free unsupervised domain adaptation: A survey. Neural Networks , 106230.

Fort, S., Ren, J., Lakshminarayanan, B., 2021. Exploring the limits of out-of-distribution detection. Advances in Neural Information Processing Systems 34, 7068–7081.

Fu, B., Cao, Z., Long, M., Wang, J., 2020. Learning to detect open classes for universal domain adaptation, in: European Conference on Computer Vision, Springer. pp. 567–583.

Ganin, Y., Lempitsky, V., 2015. Unsupervised domain adaptation by backpropagation, in: International conference on machine learning, PMLR. pp. 1180–1189.

Gao, J., Ma, X., Xu, C., 2024. Learning transferable conceptual prototypes for interpretable unsupervised domain adaptation. IEEE Transactions on Image Processing .

He, K., Zhang, X., Ren, S., Sun, J., 2016. Deep residual learning for image recognition, in: Proceedings of the IEEE conference on computer vision and pattern recognition, pp. 770–778.

Hendrycks, D., Gimpel, K., 2016. A baseline for detecting misclassified and out-of-distribution examples in neural networks, in: ICLR.

Hendrycks, D., Gimpel, K., 2017. A baseline for detecting misclassified and out-of-distribution examples in neural networks, in: International Conference on Learning Representations.

Hinton, G., Vinyals, O., Dean, J., et al., 2015. Distilling the knowledge in a neural network. arXiv preprint arXiv:1503.02531 2.

Hsu, Y.C., Shen, Y., Jin, H., Kira, Z., 2020. Generalized odin: Detecting out-of-distribution image without learning from out-of-distribution data, in: CVPR, pp. 10951–10960.

Jiang, X., Lao, Q., Matwin, S., Havaei, M., 2020. Implicit class-conditioned domain alignment for unsupervised domain adaptation, in: International Conference on Machine Learning, PMLR. pp. 4816–4827.

Jiao, W., Zhang, J., Zhang, C., 2024. Open-set recognition with long-tail sonar images. Expert Systems with Applications 249, 123495.

Kang, G., Jiang, L., Yang, Y., Hauptmann, A.G., 2019. Contrastive adaptation network for unsupervised domain adaptation, in: Proceedings of the IEEE/CVF conference on computer vision and pattern recognition, pp. 4893–4902.

Kirichenko, P., Izmailov, P., Wilson, A.G., 2020. Why normalizing flows fail to detect out-of-distribution data. NeurIPS 33, 20578–20589.

Lee, K., Lee, H., Lee, K., Shin, J., 2018a. Training confidence-calibrated classifiers for detecting out-of-distribution samples, in: ICLR.

Lee, K., Lee, K., Lee, H., Shin, J., 2018b. A simple unified framework for detecting out-of-distribution samples and adversarial attacks. NeurIPS 31.

Lee, K., Lee, K., Min, K., Zhang, Y., Shin, J., Lee, H., 2018c. Hierarchical novelty detection for visual object recognition, in: CVPR, pp. 1034–1042.

Li, J., Zhang, X., Yue, K., Chen, J., Chen, Z., Li, W., 2024. An auto-regulated universal domain adaptation network for uncertain diagnostic scenarios of rotating machinery. Expert Systems with Applications 249, 123836.

Li, X., Li, J., Zhu, L., Wang, G., Huang, Z., 2021. Imbalanced source-free domain adaptation, in: Proceedings of the 29th ACM International Conference on Multimedia, pp. 3330–3339.

Li, Y., Vasconcelos, N., 2020. Background data resampling for outlier-aware classification, in: Proceedings of the IEEE/CVF Conference on Computer Vision and Pattern Recognition, pp. 13218–13227.

Liang, S., Li, Y., Srikant, R., 2018. Enhancing the reliability of out-of-distribution image detection in neural networks, in: ICLR.

Liu, H., Cao, Z., Long, M., Wang, J., Yang, Q., 2019. Separate to adapt: Open set domain adaptation via progressive separation, in: Proceedings of the IEEE/CVF Conference on Computer Vision and Pattern Recognition, pp. 2927–2936.

Liu, L., Hospedales, T., LeCun, Y., Long, M., Luo, J., Ouyang, W., Pietikäinen, M., Tuytelaars, T., 2024. Learning with fewer labels in computer vision. IEEE Transactions on Pattern Analysis and Machine Intelligence 46, 1319–1326.

Liu, W., Wang, X., Owens, J., Li, Y., 2020. Energy-based out-of-distribution detection. NeurIPS 33, 21464–21475.

Long, M., Cao, Y., Wang, J., Jordan, M., 2015. Learning transferable features with deep adaptation networks, in: International conference on machine learning, PMLR. pp. 97–105.

Long, M., Zhu, H., Wang, J., Jordan, M.I., 2016. Unsupervised domain adaptation with residual transfer networks. Advances in neural information processing systems 29.

Long, M., Zhu, H., Wang, J., Jordan, M.I., 2017. Deep transfer learning with joint adaptation networks, in: International conference on machine learning, PMLR. pp. 2208–2217.

Lu, F., Zhu, K., Zhai, W., Zheng, K., Cao, Y., 2023. Uncertainty-aware optimal transport for semantically coherent out-of-distribution detection. arXiv preprint arXiv:2303.10449 .

Luo, Y., Guo, X., Liu, L., Yuan, Y., 2024. Dynamic attribute-guided few-shot open-set network for medical image diagnosis. Expert Systems with Applications 251, 124098.

Van der Maaten, L., Hinton, G., 2008. Visualizing data using t-sne. Journal of machine learning research 9.

Maqsood, S., Damaševičius, R., Shahid, S., Forkert, N.D., 2024. Mox-net: Multi-stage deep hybrid feature fusion and selection framework for monkeypox classification. Expert Systems with Applications 255, 124584.

Melas-Kyriazi, L., Manrai, A.K., 2021. Pixmatch: Unsupervised domain adaptation via pixelwise consistency training, in: Proceedings of the IEEE/CVF Conference on Computer Vision and Pattern Recognition, pp. 12435–12445.

Ming, Y., Sun, Y., Dia, O., Li, Y., 2023. How to exploit hyperspherical embeddings for out-of-distribution detection?, in: The Eleventh ICLR.

Mohseni, S., Pitale, M., Yadawa, J., Wang, Z., 2020. Self-supervised learning for generalizable out-of-distribution detection, in: AAAI, pp. 5216–5223.

Munro, J., Damen, D., 2020. Multi-modal domain adaptation for fine-grained action recognition, in: Proceedings of the IEEE/CVF conference on computer vision and pattern recognition, pp. 122–132.

Neal, L., Olson, M., Fern, X., Wong, W.K., Li, F., 2018. Open set learning with counterfactual images, in: Proceedings of the European Conference on Computer Vision (ECCV), pp. 613–628.

Nguyen, T., Le, T., Zhao, H., Tran, Q.H., Nguyen, T., Phung, D., 2021. Most: Multi-source domain adaptation via optimal transport for student-teacher learning, in: Uncertainty in Artificial Intelligence, PMLR. pp. 225–235.

Nguyen, T., Nguyen, V., Le, T., Zhao, H., Tran, Q.H., Phung, D., 2022. Cycle class consistency with distributional optimal transport and knowledge distillation for unsupervised domain adaptation, in: Uncertainty in Artificial Intelligence, PMLR. pp. 1519–1529.

Paszke, A., Gross, S., Massa, F., Lerer, A., Bradbury, J., Chanan, G., Killeen, T., Lin, Z., Gimelshein, N., Antiga, L., et al., 2019. Pytorch: An imperative style, high-performance deep learning library. Advances in neural information processing systems 32.

Peng, X., Bai, Q., Xia, X., Huang, Z., Saenko, K., Wang, B., 2019. Moment matching for multi-source domain adaptation, in: Proceedings of the IEEE/CVF international conference on computer vision, pp. 1406–1415.

Peng, X., Li, Y., Saenko, K., 2020. Domain2vec: Domain embedding for unsupervised domain adaptation, in: Computer Vision–ECCV 2020: 16th European Conference, Glasgow, UK, August 23–28, 2020, Proceedings, Part VI 16, Springer. pp. 756–774.

Peng, X., Usman, B., Kaushik, N., Wang, D., Hoffman, J., Saenko, K., 2018. Visda: A synthetic-to-real benchmark for visual domain adaptation, in: Proceedings of the IEEE Conference on Computer Vision and Pattern Recognition Workshops, pp. 2021–2026.

Prabhu, V., Khare, S., Kartik, D., Hoffman, J., 2021. Sentry: Selective entropy optimization via committee consistency for unsupervised domain adaptation, in: Proceedings of the IEEE/CVF International Conference on Computer Vision, pp. 8558–8567.

Rastegari, M., Ordonez, V., Redmon, J., Farhadi, A., 2016. Xnor-net: Imagenet classification using binary convolutional neural networks, in: European conference on computer vision, Springer. pp. 525–542.

Reimers, C., Runge, J., Denzler, J., 2020. Determining the relevance of features for deep neural networks, in: European Conference on Computer Vision, Springer. pp. 330–346.

Ren, C.X., Zhai, Y., Luo, Y.W., Yan, H., 2024. Towards unsupervised domain adaptation via domain-transformer. International Journal of Computer Vision , 1–21.

Ren, J., Liu, P.J., Fertig, E., Snoek, J., Poplin, R., Depristo, M., Dillon, J., Lakshminarayanan, B., 2019. Likelihood ratios for out-of-distribution detection. NeurIPS 32.

Ru, J., Tian, J., Xiao, C., Li, J., Shen, H.T., 2023. Imbalanced open set domain adaptation via moving-threshold estimation and gradual alignment. IEEE Transactions on Multimedia .

Saito, K., Kim, D., Sclaroff, S., Saenko, K., 2020. Universal domain adaptation through self supervision. Advances in neural information processing systems 33, 16282–16292.

Saito, K., Saenko, K., 2021a. Ovanet: One-vs-all network for universal domain adaptation, in: Proceedings of the ieee/cvf international conference on computer vision, pp. 9000–9009.

Saito, K., Saenko, K., 2021b. Ovanet: One-vs-all network for universal domain adaptation, in: Proceedings of the IEEE/CVF International Conference on Computer Vision, pp. 9000–9009.

Saito, K., Yamamoto, S., Ushiku, Y., Harada, T., 2018. Open set domain adaptation by backpropagation, in: Proceedings of the European Conference on Computer Vision (ECCV), pp. 153–168.

Serrà, J., Álvarez, D., Gómez, V., Slizovskaia, O., Núñez, J.F., Luque, J., 2019. Input complexity and out-of-distribution detection with likelihood-based generative models, in: ICLR.

Sicilia, A., Atwell, K., Alikhani, M., Hwang, S.J., 2022. Pac-bayesian domain adaptation bounds for multiclass learners, in: Uncertainty in Artificial Intelligence, PMLR. pp. 1824–1834.

Sun, J., Zheng, H., Diao, W., Sun, Z., Qi, Z., Wang, X., 2025. Prototype-optimized unsupervised domain adaptation via dynamic transformer encoder for sensor drift compensation in electronic nose systems. Expert Systems with Applications 260, 125444.

Sun, Y., Guo, C., Li, Y., 2021. React: Out-of-distribution detection with rectified activations. NeurIPS 34, 144–157.

Sun, Y., Li, Y., 2022. Dice: Leveraging sparsification for out-of-distribution detection, in: European Conference on Computer Vision, Springer. pp. 691–708.

Sun, Y.X., Wang, W., 2022. Exploiting mixed unlabeled data for detecting samples of seen and unseen out-of-distribution classes, in: Proceedings of the AAAI Conference on Artificial Intelligence, pp. 8386–8394.

Tan, S., Peng, X., Saenko, K., 2020a. Class-imbalanced domain adaptation: an empirical odyssey, in: Computer Vision–ECCV 2020 Workshops: Glasgow, UK, August 23–28, 2020, Proceedings, Part I 16, Springer. pp. 585–602.

Tan, S., Peng, X., Saenko, K., 2020b. Class-imbalanced domain adaptation: An empirical odyssey, in: European Conference on Computer Vision, Springer. pp. 585–602.

Tanwisuth, K., Fan, X., Zheng, H., Zhang, S., Zhang, H., Chen, B., Zhou, M., 2021. A prototype-oriented framework for unsupervised domain adaptation. Advances in Neural Information Processing Systems 34, 17194–17208.

Techapanurak, E., Suganuma, M., Okatani, T., 2020. Hyperparameter-free out-of-distribution detection using cosine similarity, in: ACCV.

Turrisi, R., Flamary, R., Rakotomamonjy, A., Pontil, M., 2022. Multi-source domain adaptation via weighted joint distributions optimal transport, in: Uncertainty in Artificial Intelligence, PMLR. pp. 1970–1980.

Tzeng, E., Hoffman, J., Zhang, N., Saenko, K., Darrell, T., 2014. Deep domain confusion: Maximizing for domain invariance. arXiv preprint arXiv:1412.3474 .

Ullah, I., An, S., Kang, M., Chikontwe, P., Lee, H., Choi, J., Park, S.H., 2024. Video domain adaptation for semantic segmentation using perceptual consistency matching. Neural Networks 179, 106505.

Vellido, A., Lisboa, P.J., Vaughan, J., 1999. Neural networks in business: a survey of applications (1992–1998). Expert Systems with applications 17, 51–70.

Venkateswara, H., Eusebio, J., Chakraborty, S., Panchanathan, S., 2017a. Deep hashing network for unsupervised domain adaptation, in: Proceedings of the IEEE conference on computer vision and pattern recognition, pp. 5018–5027.

Venkateswara, H., Eusebio, J., Chakraborty, S., Panchanathan, S., 2017b. Deep hashing network for unsupervised domain adaptation, in: Proceedings of the IEEE conference on computer vision and pattern recognition, pp. 5018–5027.

Vernekar, S., Gaurav, A., Abdelzad, V., Denouden, T., Salay, R., Czarnecki, K., 2019. Out-of-distribution detection in classifiers via generation. arXiv preprint arXiv:1910.04241 .

Vyas, A., Jammalamadaka, N., Zhu, X., Das, D., Kaul, B., Willke, T.L., 2018. Out-of-distribution detection using an ensemble of self supervised leave-out classifiers, in: ECCV, pp. 550–564.

Wang, Z., Li, L., Zeng, C., Dong, S., Sun, J., 2025. Slbdetection-net: Towards closed-set and open-set student learning behavior detection in smart classroom of k-12 education. Expert Systems with Applications 260, 125392.

Xie, M., Li, S., Gong, K., Wang, Y., Huang, G., 2024. Adapting across domains via target-oriented transferable semantic augmentation under prototype constraint. International Journal of Computer Vision 132, 1417–1441.

Yahia, M., Mahmod, R., Sulaiman, N., Ahmad, F., 2000. Rough neural expert systems. Expert Systems with Applications 18, 87–99.

Yang, Y., Gao, R., Xu, Q., 2022a. Out-of-distribution detection with semantic mismatch under masking, in: ECCV, Springer. pp. 373–390.

Yang, Y., Wang, H., Katabi, D., 2022b. On multi-domain long-tailed recognition, imbalanced domain generalization and beyond, in: European Conference on Computer Vision, Springer. pp. 57–75.

Yang, Y., Yang, X., Sakamoto, T., Fioranelli, F., Li, B., Lang, Y., 2022c. Unsupervised domain adaptation for disguised-gait-based person identification on micro-doppler signatures. IEEE Transactions on Circuits and Systems for Video Technology 32, 6448–6460.

Yao, Y., Chen, B., Liu, C., Feng, C., Gao, X., Gu, Y., 2024. Open-set adversarial domain match for electronic nose drift compensation and unknown gas recognition. Expert Systems with Applications 250, 123757.

You, K., Long, M., Cao, Z., Wang, J., Jordan, M.I., 2019. Universal domain adaptation, in: Proceedings of the IEEE/CVF conference on computer vision and pattern recognition, pp. 2720–2729.

Yu, Q., Aizawa, K., 2019. Unsupervised out-of-distribution detection by maximum classifier discrepancy, in: ICCV, pp. 9518–9526.

Zaeemzadeh, A., Bisagno, N., Sambugaro, Z., Conci, N., Rahnavard, N., Shah, M., 2021. Out-of-distribution detection using union of 1-dimensional subspaces, in: CVPR, pp. 9452–9461.

Zendel, O., Schörghuber, M., Rainer, B., Murschitz, M., Beleznai, C., 2022. Unifying panoptic segmentation for autonomous driving, in: CVPR, pp. 21351–21360.

Zhang, R., Zhang, W., Fang, R., Gao, P., Li, K., Dai, J., Qiao, Y., Li, H., 2022. Tip-adapter: Training-free adaption of clip for few-shot classification, in: European Conference on Computer Vision, Springer. pp. 493–510.

Zhang, T., Lin, J., Jiao, J., Li, H., 2024. Cross-domain data fusion generation: A novel composite label-guided generative solution for adaptation diagnosis. Knowledge-Based Systems 301, 112284.

Zhang, Y., Deng, B., Tang, H., Zhang, L., Jia, K., 2020. Unsupervised multi-class domain adaptation: Theory, algorithms, and practice. IEEE Transactions on Pattern Analysis and Machine Intelligence 44, 2775–2792.

Zhou, Y., 2022. Rethinking reconstruction autoencoder-based out-of-distribution detection, in: CVPR, pp. 7379–7387.

Zhou, Z., Guo, L.Z., Cheng, Z., Li, Y.F., Pu, S., 2021. Step: Out-of-distribution detection in the presence of limited in-distribution labeled data. NeurIPS 34, 29168–29180.